Coherent ion dip spectroscopy of the ground state benzene−Ar complex: Vibration−rotation levels up to 130 cm^{-1} intermolecular energy

R. Sussmann,[a] R. Neuhauser, and H. J. Neusser

Institut für Physikalische und Theoretische Chemie, Technische Universität München, Lichtenbergstrasse 4, D-85748 Garching, Germany

Coherent ion dip spectroscopy (CIS) provides high sensitivity and high resolution for the investigation of vibrational overtones in molecular electronic ground states. For a special time sequence of two coherent narrow-band Fourier transform limited nanosecond UV light pulses, with a modest delay of the pump pulse of 6.4 ns, a complete blocking of the population transfer to the upper state is achieved in the lambda-type three-level system ion dip experiment. This leads to ion dips with a depth as large as 95% and each dip represents an individual rovibronic transition. In this work, CIS is applied for the first time to a weakly bound van der Waals complex, benzene−Ar. We are able to observe six new van der Waals vibrational states up to an excess energy of 130 cm^{-1}. The assignments are made by comparison with recent S_1 excited state data of benzene−Ar and p-difluorobenzene−Ar and by analysis of the positions and intensities of the observed individual rotational lines. The frequency positions of the intermolecular vibrational states display a regular pattern up to 130 cm^{-1}. © *1995 American Institute of Physics.*

I. INTRODUCTION

Most of the information on van der Waals complexes of aromatic molecules originates from the first (S_1) electronic state rather than from ground (S_0) state spectroscopy. In the UV spectral region, a variety of experimental techniques has been developed particularly suitable for the investigation of weakly bound complexes produced in a cold molecular beam by detection of electronic transitions.[1−6] Among these, Doppler-free techniques led to rotational resolution and thus to the highest precision. In this way, not only the precise structure of aromatic molecule complexes with one[7−11] or two[12−15] noble gas atoms was found but also information about the van der Waals potential through the detection of van der Waals vibronic states.[16,17]

The experimental situation is in contrast to the present status of the theoretical research. *Ab initio* calculations were mainly performed for the electronic ground state since at present there is no realistic possibility to include excited electronic configurations. Though no large difference between ground and excited electronic state data of van der Waals complexes is expected, precise experimental information on the energetic position and the rotational constants of quantum states in the S_0 state van der Waals potential is highly desirable. Up to now, direct excitation of van der Waals states by far infrared techniques has been limited to van der Waals complexes of smaller molecules.[18−20] For complexes of aromatic molecules, UV techniques with the possibility of mass-selective detection, such as stimulated Raman spectroscopy[21,22] and stimulated emission pumping (SEP),[23,24] have been used for the investigation of intermolecular vibrational states. For the given sensitivity and the limited spectral resolution of these techniques only the low-

est van der Waals vibrational states have been detected in most cases.

In this work, we apply the technique of coherent ion dip spectroscopy (CIS) which was recently developed in our group[25] to investigate vibrational overtones in the van der Waals potential of the ground state (S_0) benzene−Ar complex the geometry of which was determined earlier from rotationally resolved spectra in the UV[10] and microwave spectral region.[26,27] CIS is based on the coherent interaction of two Fourier-transform limited narrow-band light pulses with a three-level system consisting of a ground state S_0 rotational level, a selected rovibronic excited state level, and a final rovibrational level in the S_0 ground state of the molecule or complex. This excitation scheme is formally equivalent to that of a stimulated emission pumping (SEP) experiment leading to a decrease of population of the upper state (populated by the pump laser) when the second (dump) laser is in resonance with the down transition. The population in the upper level is often monitored by an ionization step from the upper level to the ionization continuum. A decrease of upper state population leads to a dip in the ion current (ion dip spectroscopy)[28,29] when the dump laser is scanned in frequency. The main difference between a conventional ion dip experiment and the new coherent ion dip spectroscopy is the frequency width (coherence length) of the laser pulses and the different time sequence of the pump and the dump pulses. The first CIS experiments on benzene with pulses of 100 MHz bandwidth (FWHM) have shown that a population of the upper state can be totally suppressed leading to nearly 100% ion dips.[25] This was theoretically explained by a density matrix formalism considering the coupling of the three levels by a coherent pulsed light field.[25,30] Both the high sensitivity and the high resolution of the CIS method leading to resolved rotational states in benzene make it an excellent tool for the sensitive detection of weak rotationally resolved transitions to overtones of intermolecular vibrational states in the electronic (S_0) ground state of van der Waals complexes.

[a]Present address: Fraunhofer Institut für Atmosphärische Umweltforschung Kreuzeckbahnstr. 19, D-82467 Garmisch-Partenkirchen, Germany.

We have performed CIS experiments on the prototype van der Waals complex benzene–Ar (C_{6v}). In this complex, there exist three van der Waals vibrations, two of which (bending, $b_{x,y}$) are degenerate and of symmetry e_1 while the third one (stretching, s) is totally symmetric (a_1). The bending and stretching vibration can be excited in the S_1 state in addition to the allowed perpendicular 6_0^1 transition. While the stretching vibration of total symmetry (a_1) forms progressions of the 6_0^1 transition, additional excitation of the degenerate bending vibration requires a second-order Herzberg–Teller transition with a parallel band structure. As Van der Avoird pointed out in recent work, the A_1 and the A_2 components of the 6^1b^1 state can couple leading to a distorted rotational structure of the band which makes the analysis and assignment a difficult task.[31] The situation is much easier in p-difluorobenzene–Ar (pDFB–Ar) due to a lifting of the degeneracy of the bending mode. In recent work, we measured the electronic $S_1 \leftarrow S_0$ origin[11] and various van der Waals bands up to 125 cm^{-1} intermolecular energy in S_1 with rotational resolution.[17] We presented an assignment of the first short in-plane bending van der Waals vibration b_y on the basis of the analysis of its rotational structure. This is of a type and differs from the parallel c-type structure of the origin and the bands containing the excitation of totally symmetric stretching vibrations or even overtones of bending vibrations. The a-type rotational structure proves a Herzberg–Teller induction of the transition by the bending b_y vibration. It demonstrates the possibility of a Herzberg–Teller induction by van der Waals vibrations which has been theoretically proposed by Menapace et al.[2] Recently, an explanation for the induction of an electronic transition by a van der Waals mode based on mechanical effects was given in Ref. 22. This model explains the intensity of the bending vibration in benzene–Ar in a plausible way. Since the short in-plane bending vibration b_y of pDFB–Ar does not include a motion of the F atoms in the vibrational mode, its frequency is expected to be close to the frequency of the degenerate bending mode of benzene–Ar and results obtained for this mode in pDFB–Ar can be transferred to benzene–Ar.

In this work we present rotationally resolved CIS spectra of various intermolecular states in the ground electronic (S_0) state of benzene–Ar. For the first time overtones up to an excess energy of 130 cm^{-1} are detected. An assignment is found by comparison with recent S_1 data of pDFB–Ar and benzene–Ar and by a rotational analysis. The states at lower excess energy are compared with recent theoretical results of ab initio calculations from the literature.[31]

II. THE PRINCIPLE OF COHERENT ION DIP SPECTROSCOPY (CIS)

A. Analytical description

The excitation scheme of the three-level lambda-type process is shown in Fig. 1. It includes a (pump) laser frequency $h\nu_1$ in resonance with the transition from a ground initial state $|1\rangle$ to an excited intermediate state $|2\rangle$ and a second (dump) laser frequency ν_2 in resonance with a transition from the intermediate state down to a lower final state $|3\rangle$. This is formally identical to the excitation scheme in stimu-
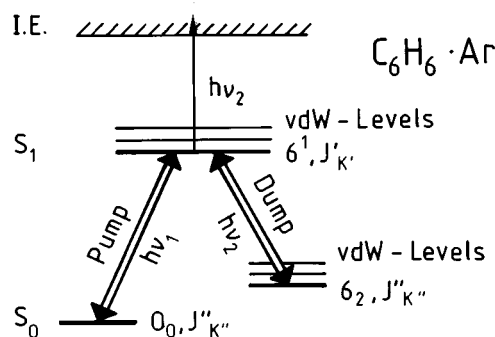

FIG. 1. Excitation scheme for stimulated emission pumping (SEP) and coherent ion dip spectroscopy (CIS) of single rovibrational levels in the ground S_0 and the excited S_1 electronic state of benzene–Ar. J and K are the rotational quantum numbers and l describes the vibrational angular momentum of the degenerate 6^1 state with one quantum of the ν_6 vibration excited in the S_1 electronic state. The terms pump ($h\nu_1$) and dump ($h\nu_2$) laser of an SEP experiment are also used for the CIS experiment. Note the differing time sequences of the pump and the dump pulses in the SEP and CIS experiments as described in the text and shown in Figs. 2 and 3.

lated emission pumping (SEP) experiments.[32,33] The population of the intermediate state is measured as a function of the dump laser frequency ν_2, e.g., by recording the ion current produced by the absorption of a second photon of the dump laser (Fig. 1) (ion dip spectroscopy[28,29]). In this way, ground state vibrational levels can be detected. In a conventional SEP-ion dip process, a resonant dump transition leads to a depopulation of the excited level and to a dip in the ion current at the resonance frequency, the depth of which can be 50% at most when the dump transition is saturated.

When the three-level system is driven in a coherent manner a complete suppression of the population transfer to the intermediate level can be achieved either by a complete population transfer to the final state[37–39] or a complete blocking of the population transfer.[25] The latter led to nearly 100% dips in the ion current in a CIS experiment. The following conditions have to be fulfilled for this special population dynamics: (i) An effective three level system has to be realized consisting of selected pure rovibrational and rovibronic states, respectively. For model systems of the size of benzene–Ar this requires a spectral resolution which can be achieved by pulsed amplification of a cw single mode dye laser[34] (see below) in combination with the reduced rotational level density and the reduced Doppler width in a skimmed cold supersonic beam. (ii) Vanishing phase fluctuations of the pump and dump pulses are required as given for nearly Fourier transform limited pulses. Laser intensities must be sufficiently high, so that the Rabi frequencies of the two transitions exceed the rate of the intramolecular or radiative relaxation processes. (iii) In order to suppress any population transfer to the intermediate upper state level $|2\rangle$ (Fig. 1), the coherent process requires a special time sequence of the two ns laser pulses with a leading edge of the dump pulse. In addition to the exact numerical calculation of the population dynamics in a density matrix approach presented below (Sec. II B), two limiting analytical descriptions, i.e., a trapping process or level shifting by the dynamic Stark effect may be considered.

In an effective lambda-type three level scheme two rovibrational ground state levels $|1\rangle$ and $|3\rangle$ are coupled via two resonant laser transitions with ν_1 and ν_2 to one upper (rovibronic) level $|2\rangle$ (Fig. 1). This can lead to a trapping process,[35] i.e., the total system including molecular states and the two light fields is in the "trapped state" which is a linear superposition of the two levels $|1\rangle$ and $|3\rangle$, without any contribution from the upper level $|2\rangle$. In the CIS process, the system is instantaneously *forced* into the trapped state by a special time sequence of the two laser pulses with a leading edge of the *dump* pulse. There is only one additional condition, namely the *adiabatic evolution* of the system[36] in order to keep the system in the trapped state and thus suppressing any population transfer to the intermediate state (rovibronic level $|2\rangle$). During the subsequent evolution, the relative contribution of the two ground state levels within the trapped state is controlled by the relative value of the Rabi frequencies of the pump and the dump transitions. For practical reasons in CIS experiments, a maximum overlap of the dump and pump pulses is necessary, in order to achieve a strong and stable ion current by resonant ($h\nu_1 + h\nu_2$)-absorption when the dump laser frequency ν_2 is off resonance (Fig. 1). This pulse sequence yields a population dynamics[25] which is completely different from that of population transfer experiments.[37–39] As will be shown below by density matrix calculations the maximum overlap results in a trapping of population in the initial state $|1\rangle$ and no transfer to the final state $|3\rangle$. A population transfer to the final state is possible with pulsed lasers as demonstrated in recent stimulated Raman adiabatic passage (STIRAP) experiments with the diatomic molecule NO.[39] The STIRAP technique requires a different time sequence with a stronger delay of the pump pulse from the dump pulse, a remaining small overlap of both pulses and a dominating falling edge of the pump laser at the end of the interaction time. In a similar manner effective population transfer to a final upper state was achieved in ladder type systems.[40,41]

For the conditions of our experiment, i.e., a strong dump laser and a relatively weak pump laser intensity the interruption of the resonant ionization path $|1\rangle \rightarrow |2\rangle \rightarrow |$ continuum$\rangle$ can be described in a different way, namely, by a dynamic (AC) Stark shift of levels $|2\rangle$ and $|3\rangle$ in the strong resonant ($|2\rangle \leftrightarrow |3\rangle$) dump field. The high Rabi frequency of the dump laser leads to an AC Stark shift of level $|2\rangle$ which exceeds the linewidth of the pump laser (100 MHz). Thus, the pump transition $|1\rangle \leftrightarrow |2\rangle$ is no longer in resonance and the ion current breaks down. Again, the leading edge of the dump laser pulse is necessary to provide the shift of level $|2\rangle$ before the pump laser interaction starts. However, within this picture as an approximation for the limit of two laser pulses with strongly differing intensity it is not necessary for the Rabi frequency of the pump transition to exceed the rate of the intramolecular or radiative relaxation process, and no adiabatic evolution of the system as in STIRAP experiments is required.

Both analytical descriptions may be considered as limiting cases which may be chosen depending on the conditions of a real experiment. The conditions of a CIS experiment appear to be closer to the situation where the dynamic Stark
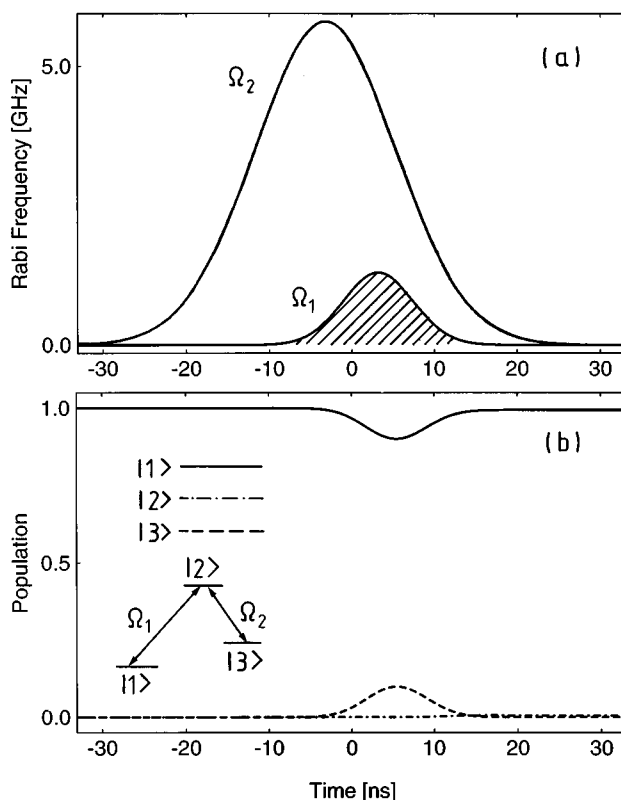

FIG. 2. (a) Time evolution of the Rabi frequencies Ω_1, Ω_2 simulating the typical time sequence of the dump and pump pulses in a CIS experiment. (b) Population of the levels $|1\rangle$, $|2\rangle$, and $|3\rangle$ (see inset) as a function of time numerically calculated from the density matrix equations in the rotating wave approximation for the Rabi frequencies given in (a). A small amount of transient population is transferred from level $|1\rangle$ to level $|3\rangle$ and then transferred back to level $|1\rangle$. No transient population in level $|2\rangle$ is found.

picture is more appropriate. However, rather than favoring one model, we decided to solve the density matrix equations numerically for an exact simulation of the population dynamics (see below).

B. Population dynamics

For simulation of the population dynamics in CIS experiments, we performed numerical calculations solving the density matrix model equations[42] for a three level system with different Rabi frequencies for the pump and the dump transition, assuming no phase fluctuations in the laser pulses (i.e., Fourier transform limited laser pulses) and neglecting the ionization step. In Figs. 2 and 3, the calculated results for the population of the initial level $|1\rangle$, the excited level $|2\rangle$ and the final level $|3\rangle$ are shown for two different pulse delays as a function of time. For illustration of the time delay, the instantaneous Rabi frequencies Ω_1 and Ω_2 of the pump and dump pulses, respectively, are depicted as a function of time in Figs. 2(a) and 3(a), respectively. The peak values used are $\Omega_1^{max} = 1.3$ GHz and $\Omega_2^{max} = 5.8$ GHz.

For the pulse sequence of Fig. 2, the delay of the peak maxima is 6.4 ns and corresponds to the experimental value of the CIS experiment in this work. From Fig. 2(a), it is clearly seen that the leading edge of the dump pulse arises first and thus one important condition for a coherent process
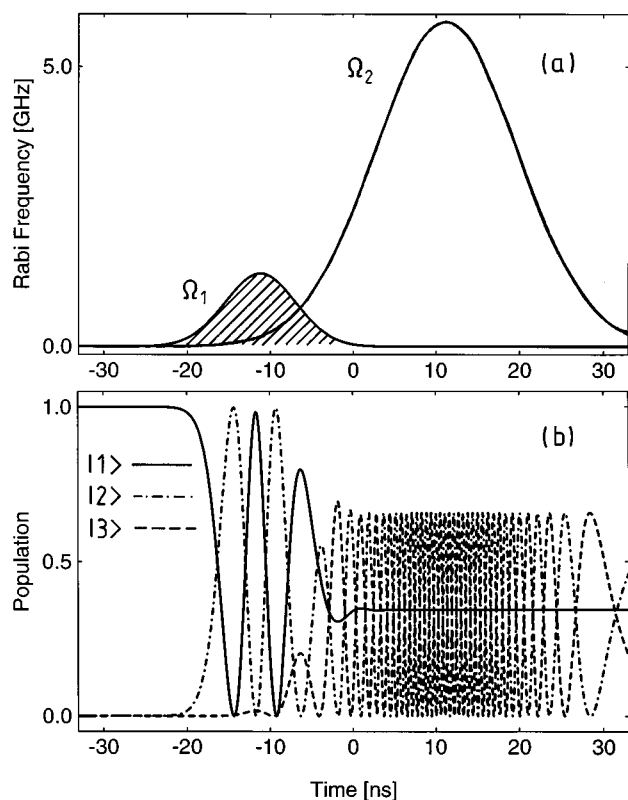
FIG. 3. (a) Time evolution of the Rabi frequencies Ω_1, Ω_2 for a conventional SEP configuration with a delayed dump pulse. (b) Population of the levels $|1\rangle$, $|2\rangle$, and $|3\rangle$ as a function of time numerically calculated from the density matrix equations in the rotating wave approximation for the Rabi frequencies in (a). Complicated transient oscillations of the population of all levels with a resulting population in the upper level $|2\rangle$ and incomplete suppression of the ionization path is found leading to less deep ion dips.

leading to ionization suppression (see above) is fulfilled. In this case, a small part of the population of the ground state level $|1\rangle$ is directly transferred to the final state $|3\rangle$ to be subsequently transferred back to the initial state during the pulse overlap without any noticeable population in the excited level $|2\rangle$ even though the pump laser frequency ν_1 is in resonance with the $|2\rangle \leftarrow |1\rangle$ transition. From the result in Fig. 2(b), it is concluded that no population is monitored in the excited level when the dump laser frequency ν_2 is in resonance with the transition $|2\rangle \rightarrow |3\rangle$ from the excited to the final level, thus leading to 100% ion dips. The depth of 95% observed in our experiments (Fig. 5) is close to this ideal value. In recent work, we were able to simulate the characteristic line shape in CIS (see, e.g., Fig. 5) using a density matrix approach and taking into account a spatial Gaussian intensity profile as well as the orientational distribution of the molecules (m-quantum number).[30]

For comparison, the population dynamics for the time sequence of a conventional SEP experiment is shown in Fig. 3. An oscillation of the population of the levels $|1\rangle$, $|2\rangle$, and $|3\rangle$ changing with the instantaneous Rabi frequencies can be recognized. In contrast to the CIS process (Fig. 2), level $|2\rangle$ is periodically populated. For a realistic experiment with spatial intensity distribution, Rabi oscillations with different frequencies overlap. This leads to an average population of this

level and consequently to ion dips with less than 100% depth.

C. Experiment

The scheme of the experimental setup was shown in our previous work.[25] Briefly, the pump and dump laser pulses are provided by two pulsed amplified cw lasers. The cw ring laser (Coherent 699/21) yielding the pump pulse is operated at $\lambda = 518$ nm with coumarin 102 dye. It is pumped by the multiline violet output of a Kr^+ laser (Coherent Innova 200). The cw light with a frequency width of 2 MHz is amplified in a three-stage amplifier system[34] yielding nearly Fourier transform limited light pulses with a pulse energy of 400 μJ, a width of 10 ns (FWHM) and a frequency width of 100 MHz (FWHM) after frequency doubling in a BBO crystal. The cw ring laser providing the dump pulse is pumped by the 514.5 nm line of an Ar^+ laser (Spectra Physics 171) and operated at $\lambda = 534.9$ nm with rhodamine 110 dye. The pulse energy after amplification and frequency doubling in a KDP crystal is 1 mJ for a pulse width of 20 ns (FWHM) and a frequency width of 60 MHz (FWHM). Both amplifier stages are pumped by the 300 mJ pulses ($\lambda = 308$ nm) of an excimer laser (Lambda Physik EMG 201 MSC). Pump and dump laser beams are focused down to 0.5 mm. The pump laser is attenuated by a factor of 50 to avoid absorption of a second photon from this laser resulting in an ionization of the molecule. The pump pulse is delayed by 6.4 ns from the dump pulse by an optical delay line. Both counterpropagating narrow band light pulses interact with benzene–Ar in the center of a cooled supersonic beam expanded from a reservoir with 1% benzene seeded in Ar at a backing pressure of 2 bar through a nozzle with a 300 μm diameter orifice.[43] A conical skimmer reduces the residual Doppler width below the laser linewidth. A delay of 6.4 ns of the pump laser pulse is achieved by an optical delay line. The absorption of a second dump laser photon from the excited 6^1 state results in an ionization of the complex: For the moderate inverted (compared to SEP) delay chosen in the CIS configuration sufficient intensity of the (first) dump laser pulse is present when the pump laser pulse arrives. In this way, the population in the intermediate state is probed by the absorption of a dump laser photon. The molecular ions are mass separated in a time-of-flight mass spectrometer and detected with multichannel plates. The recorded spectra were not normalized to the UV power of the lasers. There was no signal averaging over several pulses. Scanning the pump laser for a fixed nonresonant frequency of the (ionizing) dump laser and integrating the ion current at mass 118 u yields a rotationally resolved spectrum of the 6_0^1 band of benzene–Ar or of one of the vdW vibronic bands (Fig. 4, Ref. 44). The pump laser frequency is then kept constant on top of a single selected rotational line while the dump laser frequency is scanned around the expected transition down to a selected (vdW) vibrational state in the S_0 electronic ground state leading to rotationally resolved CIS spectra following the selection rules described in Sec. III A. The relative frequency of the dump laser is measured with a 150 MHz free spectral range interferometer and the absolute frequency is calibrated by the simultaneously measured fluorescence spectrum of I_2 vapor.

TABLE I. Hönl–London factors[a] of perpendicular and parallel dump transitions.

Rotational state	J''	K''	Hönl–London factor
$J'=K'=4,\ l_6'=-1$	5	5	2.0
perpendicular	5	3	0.04
	4	3	0.4
	3	3	1.56
$J'=K'=4,\ l_6'=-1$	5	4	0.2
parallel	4	4	0.8

[a]Calculated according to Ref. 55.

III. RESULTS

A. Symmetry and selection rules

For an analysis of observed down transitions it is necessary to discuss which transitions can be expected from symmetry selection rules. In harmonic approximation point group C_{6v} is adequate to derive the selection rules for vibronic transitions in benzene–Ar. For the assignment of the CIS spectra presented below, we discuss the selection rules for dump transitions to vdW rovibrational states starting from the $J'=K'=4,\ l_6'=-1$ rotational levels in the vdW vibronic states 6^1, 6^1s^1, and $6^1b^2(l_b'=0)$ of symmetry species E_1 that are excited by the pump laser. Here J and K are the rotational quantum numbers of a symmetric top and s and b denote the intermolecular stretching and bending modes, respectively; the ν_6 vibrational angular momentum with the quantum number l_6 causes a splitting of each rotational substate in the degenerate 6^1 and 6_2 (see below) vibronic states due to Coriolis coupling;[45] l_b is the vibrational angular momentum resulting from the degenerate vdW bending modes.

The dump laser frequency is in resonance with the $6^1(J'=K'=4,+l)\rightarrow 6_2(J''=K''=3)$ transition (Fig. 1) which is induced by vibronic interaction through the ν_6 skeletal mode. The threefold degenerate 6_2 ground state has symmetry A_1+E_2 and is split in $A_1(l_6''=0)$ and $E_2(l_6''=\pm2)$, respectively, with differing (skeletal) vibrational angular momentum.[46] Both components are accessible by perpendicular transitions from the S_1 rovibronic states given above. The selection rules for the $(\pm l)$ label[47] together with $\Delta J=0,\ \pm1$ und $\Delta K=\pm1$ lead to four allowed transitions to the J'', K'', $l_6'' = (5,5,-2)$, (5,3,0), (4,3,0), and (3,3,0) states with the relative intensities given by the Hönl–London factors of the individual transitions (Table I). These selection rules are also valid for dump transitions to the 6_2s_1, $6_2b_2(l_b''=0)$, 6_2s_2, $6_2s_1b_2(l_b''=0)$, 6_2s_3, and $6_2b_4(l_b''=0)$ vdW vibrational states.

A different situation has to be considered for transitions to the sixfold degenerate 6_2b_1, $6_2b_1s_1$, or 6_2b_3 vdW vibrational states with $B_1+B_2+2E_1$ symmetry. Transitions to these states are *not* electronically symmetry allowed from the upper 6^1, 6^1s^1, or 6^1b^2 states. However, the *vibronic* symmetry condition includes the possibility to reach the E_1 states via *parallel* ($\Delta K=0$) transitions. In this case, intensity is induced by second-order Herzberg–Teller coupling via the induced transition moment
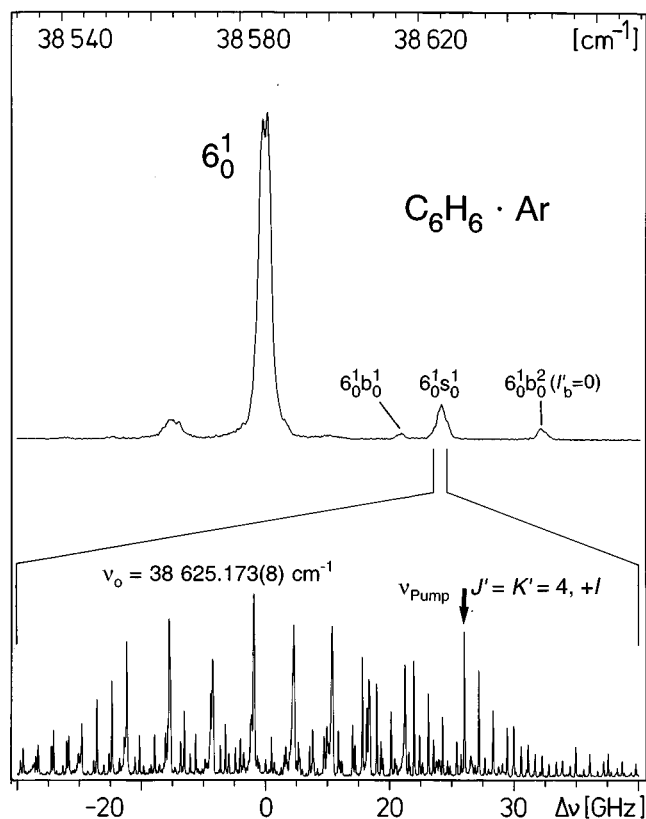

FIG. 4. Upper trace: Low resolution vibrationally resolved vibronic spectrum of the benzene–Ar complex measured by resonance-enhanced two-photon ionization. Note the three weak vdW vibronic bands to the blue of the Herzberg–Teller induced 6_0^1 origin which include the additional excitation of the vdW bending mode b and the vdW stretching mode s. Lower trace: Rotationally resolved spectrum of the $6_0^1s_0^1$ band. The $J'=K'=4,\ +l$ rotational line indicated by an arrow was selected for the recording of the CIS spectrum shown in Fig. 5.

$$\left(\frac{\partial^2 \mathbf{R}_e}{\partial Q_6 \partial Q_{\text{bend}}}\right)_{\text{eq}} Q_6 Q_{\text{bend}}, \qquad (1)$$

containing the derivative of the electronic transition moment $\mathbf{R}_e$ with respect to Q_6 and Q_{bend}. Here Q_6 is the ν_6 skeletal normal coordinate, Q_{bend} is the vdW bending normal coordinate, "eq" designates the equilibrium configuration. The fourfold degenerate $2E_1$ states are split into the vibrational angular momentum components $l_6'', l_b'' = (0,\pm1)$ and $(\pm2,\pm1)$, respectively.[46] Only the $[l_6'', l_b'' = (0,+1)$ and $(-2,-1)]$ states are allowed in a parallel transition according to the $(\pm l)$-label selection rule. This is also valid for the allowed $6_2b_1s_1$ rovibrational states. Similarly, only transitions to the $l_6'', l_b'' = (0,+3)$, and $(-2,-3)$ rotational sublevels in the the 6_2b_3 vibrational state are possible. The respective Hönl–London factors are listed in Table I. With these selection rules in mind we are able to find an assignment of the observed peaks in the CIS spectra presented below.

B. CIS spectra of high vdW vibrational quantum states in the S_0 intermolecular potential

The recording of rotationally resolved ground state spectra in benzene–Ar with the CIS double resonance technique
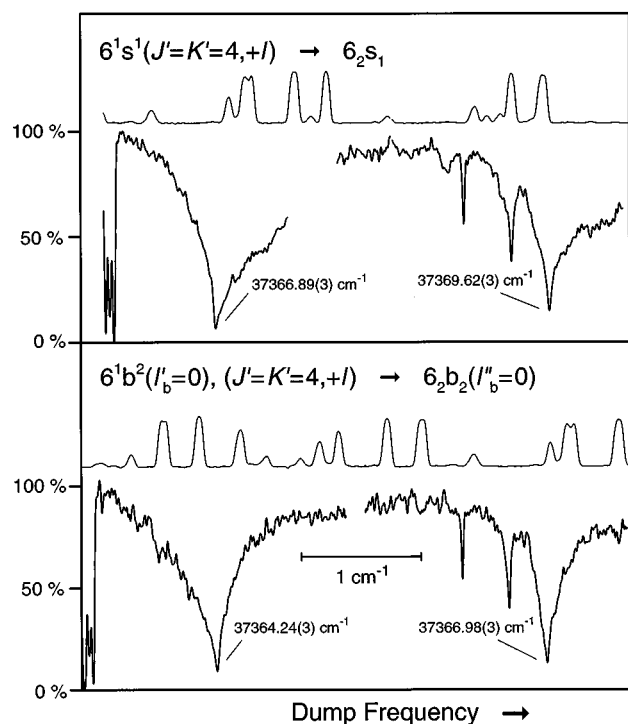
FIG. 5. Coherent ion dip (CIS) spectra of the $6_2 s_1$ and $6_2 b_2(l''_b = 0)$ states in benzene–Ar with the $J' = K' = 4$, $+l$ rotational levels of the $6^1 s^1$ and $6^1 b^2(l'_b = 0)$ vibronic levels used as upper intermediate state levels, respectively; relative transition strengths are given by the Hönl–London factors listed in Table I. The iodine spectra displayed on top were synchronously recorded for absolute frequency calibration.

requires a detailed understanding of the rotational structure of the vibronic and vdW vibronic bands in the S_1 state of the complex[4,44] (see Fig. 4) used as an upper intermediate state for the CIS process. Rotational lines representing individual rovibronic transitions must be selected in order to define the initial state and the intermediate upper state in the effective three-level system. The (vdW) rovibronic line structure in benzene–Ar is more condensed than in the 6^1_0 band of the benzene monomer. For this reason, it is difficult to tune the pump laser frequency to a specific identified rotational line and keep the laser frequency fixed on top of the line during the scan of the dump laser frequency. It was possible to unambiguously select the relatively strong $J' = K' = 4$, $\Delta J = \Delta K = +1$ pump transitions in the 6^1_0, $6^1_0 s^1_0$, and $6^1_0 b^2_0$ vdW vibronic bands of benzene–Ar as upper states of the lambda-type three-level system (Fig. 1).

In Fig. 5, two CIS spectra are shown resulting from a scan of the dump laser frequency with the pump laser frequency fixed at resonance with the $(J' = K' = 4, +l)$ rotational states of the $6^1 s^1$ (Fig. 4) and $6^1 b^2(l'_b = 0)$ vdW vibronic states. The spectra were detected at intermolecular energies (relative to the position of the 6_2, S_0 state) which are close to the respective intermolecular energies of the corresponding vdW vibronic states in the S_1 electronic state. In agreement with the rotational selection rules derived in Sec. III A, four rotational dump transitions are found in each case at the frequency positions listed in Table II. The strongest dump transitions lead to dips with 95% depth (Fig. 5). This is similar to the CIS spectra of the benzene monomer[25] and

represents a characteristic feature of the coherent process. The broad width of the deep ion dips is due to a saturation and the special shape was explained using a density matrix approach taking into account a spatial Gaussian intensity profile as well as the orientational distribution of the molecules (m-quantum number) in our recent work.[30] In the displayed spectra, two weaker dips are seen resulting from smaller Hönl–London factors (Table I) of these transitions as has been shown in the SEP[49] and CIS[25] spectra of bare benzene in our previous work. All dump transitions are schematically displayed in Fig. 6.

Up to now, only three vdW vibronic states have been detected in the vdW vibronic $S_1 \leftarrow S_0$ spectrum of benzene–Ar both from low (vibrational)[2] and high (rotational) resolution experiments (Fig. 4).[4,44] In Fig. 6, we demonstrate that we were able to detect a large number of vdW vibrational quanta at high energy in the S_0 state with the CIS method. This demonstrates the high sensitivity of the method. Now we discuss the measured vdW rovibrational spectra in detail.

1. 6_2 state

The $6^1 \leftarrow 6_2$ transition without additionally excited vdW states was chosen as a starting point. The frequencies of the rotational dump transitions in the CIS spectrum (Fig. 5) can be described by the energy formula for a symmetric top[50] (Table I). Since the difference between the rotational constants $A''_v - A''_0$ and $B''_v - B''_0$ is small compared to the accuracy of the frequency scale in the experiment (≈ 300 MHz), we use the constants A''_0 and B''_0 to calculate final state positions in the electronic ground state.[10] Using this approximation, the effective Coriolis coupling constant ζ''_{eff} and the rotationless origins G_0 of the $6_2(l''_6 = 0)$ and $6_2(l''_6 = \pm 2)$ states split by the vibrational–angular momentum are derived from the experimental frequency positions. With $\zeta''_{\text{eff}} = -2\zeta''_6 = -1.15$ (Ref. 48) the two rotationless origins $G_0(6_2, l''_6 = 0) = 1215.93(3)$ cm^{-1} and $G_0(6_2, l''_6 = \pm 2) = 1215.96(3)$ cm^{-1} result, respectively.

2. $6_2 b_1$ state at $6_2 + 32.8$ cm^{-1}

The rotationally resolved CIS spectrum of this state has been recorded starting from a selected rotational level in a S_1 vdW vibronic level which is located 31.164 cm^{-1} to the blue of the 6^1 state. The assignment as the $6_2 b_1$ state results from a comparison with different high and low resolution measurements: (i) in pDFB–Ar we found experimental proof for the assignment of the short in-plane bending mode with a fundamental frequency of 34 cm^{-1} in the S_1 state.[16] From a kinematic point of view, i.e., considering the vdW bending mode as a *librational* motion,[51,22] we concluded that the *short* in-plane bending mode in pDFB–Ar has a frequency which nearly equals that of the bending mode in benzene–Ar since the former does not include a motion of the heavy fluorine atoms. This is evidence for the assignment of the vdW vibronic band at 31.164 cm^{-1} in benzene–Ar (see above) as the $6^1_0 b^1_0$ band. (ii) In recent work the rotational spectrum of this vdW vibronic band in benzene–Ar[44] was

TABLE II. Rovibrational assignments in the CIS spectra of benzene–Ar.

S_1	$S_0: E/cm^{-1}$ (exp.)	Vib.	J''	K''	l_6'', l_b''	$\delta\nu''_{vdW}/cm^{-1}$
6^1,	1216.89(3)	6_2	3	3	0	0
	1217.21(3)		4	3	0	
$J'=K'=4, l_6'=-1$	1217.60(3)		5	3	0	
	1219.62(3)		5	5	-2	
$6^1 b^1$	1249.68(3)	$6_2 b_1$	-	-	-	32.8[b]
	1249.79(3)		-	-	-	
J', K', l_6', l_b'	1250.09(3)		-	-	-	
not determined	1251.18(3)		-	-	-	
	1251.51(3)		-	-	-	
$6^1 s^1$,	1256.89(3)	$6_2 s_1$	3	3	0	39.99(30)
	1257.19(3)		4	3	0	
$J'=K'=4, l_6'=-1$	1257.58(3)		5	3	0	
	1259.61(3)		5	5	-2	
$6^1 b^2$,	1282.30(3)	$6_2 b_2$	3	3	0,0	65.39(3)
	1282.61(3)		4	3	0,0	
$J'=K'=4, l_b'=-1,$	1282.98(3)		5	3	0,0	
$l_b'=0$	1285.05(3)		5	5	-2,0	
$6^1 s^1$,	1294.03(3)	$6_2 s_2$	3	3	0	77.11(3)
	1294.33(3)		4	3	0	
$J'=K'=4, l_6'=-1$	...[a]		-	-	-	
	1296.75(3)		5	5	-2	
$6^1 s^1, J'=K'=4,$	1312.93(3)	$(6_2 b_3)$	(4	4	0,+3)	(95.62(3))
$l_6'=-1$	1315.69(3)		(5	4	-2,-3)	
		or				or
$6^1 b^2, J'=K'=4,$	1312.92(3)	$6_2 s_1 b_2$	3	3	0,0	96.03(3)
$l_6'=-1, l_b'=0$	1315.68(3)		-	-	-	
			-	-	-	
			5	5	-2,0	
$6^1 s^1$,	...[a]	$6_2 s_3$	-	-	-	117.17(3)
	...[a]		-	-	-	
$J'=K'=4, l_6'=-1$	...[a]		-	-	-	
	1336.79(3)		5	5	-2	
$6^1 b^2$,	1345.04(3)	$6_2 b_4+$				128.2[b]
$J'=K'=4, l_6'=-1,$	1347.70(3)	combination				
$l_b'=0$	1348.15(3)					

[a]Transition is too weak to be detected.
[b]Difference between the frequencies of lowest energy rotational state and the lowest energy state in the 6_2 system.

explained assuming a parallel transition including Coriolis interaction because of the degeneracy of the bending modes.[52] (iii) From stimulated Raman spectroscopic measurements with lower (vibrational) resolution, Maxton et al.[22] found a band at about 33.5 cm^{-1} which they assigned to the bending frequency. This value is in agreement with the value of this work.

Since the rotational quantum number of the selected upper (rovibronic) level in the $6_0^1 b_0^1$ band has not been identified during the experiment, we cannot give a rotational assignment of the dips detected in the CIS experiment (Table II). However, we can state that the *inter*molecular frequency shift of the $6_2 b_1$ ground state, $\delta\nu''_{vdW} := G_0(6_2 b_1, l_6'' = 0) - G_0(6_2, l_6'' = 0) = G_0(6_2 b_1, l_6'' = -2) - G_0(6_2, l_6'' = -2)$ is significantly higher ($\delta\nu''_{vdW} \approx 32.8$ cm^{-1}) than the analogous intermolecular frequency shift $\delta\nu'_{vdW}$ of the S_1 ($6^1 b^1$) state [$\delta\nu'_{vdW} = 31.164$ cm^{-1} (Ref. 44)].

3. $6_2 s_1$ state at $6_2 + 39.99$ cm^{-1}

The peak positions in the CIS spectrum (Fig. 5) can be analyzed following the discussion for the 6_2 state (Tables I and II). The vdW *vibronic* frequency shift $\delta\nu''_{vdW} = 39.99(3)$ cm^{-1} of the resulting rotationless origin nearly equals the vdW vibronic shift in the S_1 ($6^1 s^1$) state [$\delta\nu'_{vdW} = 40.102$ cm^{-1} Ref. 44].

4. $6_2 b_2 (l_b'' = 0)$ state at $6_2 + 65.39$ cm^{-1}

The experimentally observed rotational structure of the vibronic $6_0^1 b_0^2$ band was well simulated in our previous work using $\zeta'_{eff} = -0.5734(2)$.[44] Thus it is clear that this band represents the transition to the ($l_b' = 0$) component of the

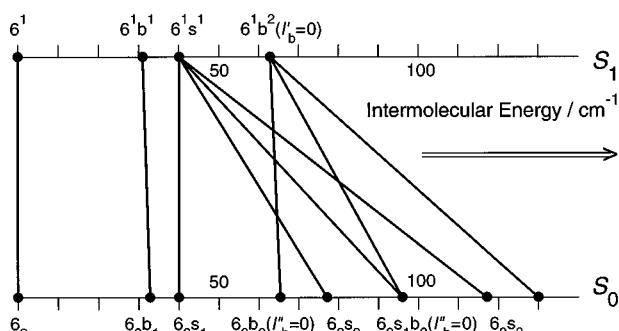FIG. 6. Scheme of vdW vibronic levels $|2\rangle$ in S_1 (intermediate state) and vdW vibrational levels $|3\rangle$ in S_0 (lower state) investigated in this work. Observed transitions are indicated by the solid lines connecting the upper and lower scales. The intermolecular energy positions represent the experimentally determined values (Table II).

FIG. 7. Excess energy of detected vdW states in S_0 of benzene–Ar as a function of excited quanta of the vdW stretching modes ($\triangledown$) and bending modes ($\bigcirc$). The solid line represents a quadratic fit to the experimental points.

$6^1 b^2$ state. The CIS spectrum (Fig. 5) starting from the $6^1 b^2 (l'_b = 0)$ state is located at roughly the same frequency as the $6^1 \rightarrow 6_2$ transitions. From this we conclude that $\Delta \mathrm{vib}_\mathrm{vdW} = 0$, i.e., there is no change in the vdW vibrational quantum number and we assign vibrational state detected in the CIS spectrum as $6_2 b_2 (l''_b = 0)$. Here we additionally used the $\Delta l = 0$ selection rule. The rotational assignment is identical to that in the CIS spectrum of the 6_2 state (Tables I and II). The resulting vdW vibrational frequency shift of the rotationless origins $\delta \nu''_\mathrm{vdW} = 65.39(3)$ cm^{-1} is slightly but significantly *higher* than the corresponding S_1 ($6^1 b^2$, $l'_b = 0$) vdW vibronic shift ($\delta \nu'_\mathrm{vdW} = 62.882$ cm^{-1} [(Ref. 44)].

5. $6_2 s_2$ state at $6_2 + 77.11$ cm^{-1}

Using the $6^1 s^1$ state as an upper state a vdW vibrational ground state at $\delta \nu''_\mathrm{vdW} = 77.11(3)$ cm^{-1} was detected. As mentioned above no state with comparable intermolecular energy could be found in the S_1 state. The detection of *more than two* rovibratoric dips in the vdW vibrational state under discussion (Table II) is proof of a perpendicular transition (see Sec. III A and Table I), i.e., the symmetry species of the excited vdW vibrational state in the S_0 electronic state is A_1. Together with the observed frequency position of 77.11 cm^{-1} to the blue of the $6^1 \rightarrow 6_2$ transition this is evidence for the assignment as $6_2 s_2$ state (Table II, Fig. 6).

6. State at $6_2 + 96$ cm^{-1}

For dump transitions leading to intermolecular energies of 96 cm^{-1} starting either from the $6^1 s^1$ or the $6^1 b^2 (l'_b = 0)$ states as upper intermediate states of the CIS process (Fig. 6, Table II) only two ion dips could be detected.

Following the symmetry selection rules discussed in Sec. III A this could be taken as an indication for a *parallel* dump transition leading e.g. to the $6_2 b_3$ state which should be located in this energy region. In this case the dip at 1312.93(3) cm^{-1} would be assigned as a dump transition to the ($J'' = K'' = 4$, $l''_6 = 0$, $l''_b = +3$) state, and the dip at 1315.69(3) cm^{-1} to the ($J'' = 5$, $K'' = 4$, $l''_6 = -2$, $l''_b = -3$) state, respectively. We found ion dips of comparable

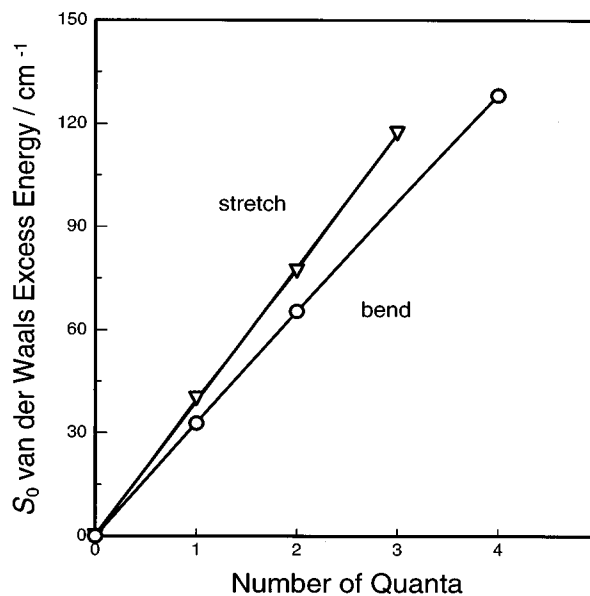intensity. This contradicts the expected intensity ratio of 4 for the two transitions expected from the strongly differing Hönl–London factors (Table I). Another argument against the assignment as a parallel transition originates from the energy positions of the dips. From the energy formula of a symmetric top with $\zeta''_6 = +0.575$ of bare benzene[48] a Coriolis coupling constant for the bending mode $\zeta''_b = +0.130$ results. This value is significantly different from the value of $\zeta'_b = +0.2117$ resulting from the fit of the rotationally resolved $6^1_0 b^1_0$ band of benzene–Ar.[44,52] Both the intensity and the energy assignment make the assignment as a parallel transition unlikely.

It is more likely that the two ion dips result from a perpendicular transition. The missing four symmetry-allowed rotational dump transitions are not detected because of their weak Hönl–London factors (Table I). This conclusion is corroborated by the frequency difference of the two observed peaks being the same as the analogous distance of the two strongest dips in the CIS spectra of the transitions leading to the 6_2, $6_2 s_1$, and $6_2 b_2 (l''_b = 0)$ states (Table II). Assuming a perpendicular transition, only combination states containing totally symmetric vdW modes can be reached from the $6^1 s^1$ and $6^1 b^2$ states. This leads us to the tentative assignment of the state at 96 m^{-1} as the $6_2 s_1 b_2 (l''_b = 0)$ state (Table II).

7. $6_2 s_3$ state at $6_2 + 117.17$ cm^{-1}

The observed single dip at a total vibrational energy of 1336.79(3) cm^{-1} (Table II) is assigned as the rotational transition with the largest Hönl–London factor of a weak perpendicular transition. The assignment to the $6_2 s_3$ state fits best to the observed vdW vibrational frequency shift of $\delta \nu''_\mathrm{vdW} = 117.17(3)$ cm^{-1} (Fig. 6).

TABLE III. Experimental and theoretical intermolecular energies.

vdW vibration	Experimental, S_1 state[a]/cm^{-1}	Experimental, S_0 state/cm^{-1}	Theoretical[b] S_0 state/cm^{-1}
$b1$	31.164	32.8	30.17
$s1$	40.102	39.99(3)	41.03
$b2(l_b=0)$	62.882	65.39(3)	64.39
$s2$	not observed	77.11(3)	79.35
$b3$	not observed	not observed	90.5
$s1b2(l_b=0)$	not observed	96.03(3)	...
$s3$	not observed	117.17(3)	...
$b4$	not observed	128.2	...

[a]Taken from Ref. 44.
[b]Taken from Ref. 31.

8. States at 6_2+128 cm^{-1}

In this frequency range, three ion dips were detected (Table II) but the frequency spacings are not consistent with the pattern of rotational transitions to only *one* vdW vibrational state. We tentatively assume that the two lowest energy ion dips represent the two strongest rotational dump transitions to the $6_2b_4(l_b''= 0)$ state.

The intermolecular energies of all vdW vibrational levels discussed above are summarized in Fig. 7 and displayed as a function of their stretching and bending vdW vibrational quantum numbers. The frequency positions seem to display a harmonic behavior. However, we would like to stress that the assignments to accurate vdW vibrational quantum numbers are only valid for the low intermolecular energy states in a linear approximation. For higher intermolecular energies mixing of intermolecular bend and stretch motion has to be taken into account as demonstrated recently by the analysis of vibration–rotation coupling in the high energy vdW modes of pDFB–Ar.[17]

IV. DISCUSSION AND CONCLUSION

In Table III, the vdW vibrational frequency shifts of the ground (S_0) state obtained from coherent ion dip spectroscopy (CIS) in this work are summarized and compared to the vdW *vibronic* frequency shifts of the S_1 state derived in our recent work from rotationally resolved REMPI spectra.[44] In addition, theoretical vdW vibrational frequencies from three-dimensional (3D) quantum mechanical calculations[31] are listed. It is clearly seen that S_0 and S_1 vdW vibrational frequencies do not differ very much. Nearly no change of the fundamental vdW stretching frequency is detectable from our experiment (Table II, Fig. 6). However, the fundamental bending frequency in the S_0 state is higher than in the S_1 state by ≈ 1.5 cm^{-1} or 4%. This difference may have two different reasons: (i) The different intramolecular vibrational energies of the 6^1 and 6_2 states excited in combination with the vdW mode or (ii) differences in the intermolecular potential of the electronic ground and excited states. We exclude the former mechanism since the stretching frequency was found to be unchanged (see above). At first sight, different vdW potentials with a somewhat stronger binding energy in the S_1 state (~ 21 cm^{-1}) should result in *increasing* intermolecular frequencies in the S_1 state. The observed *decrease* of the vdW bending frequency upon electronic excitation *and*

the nearly unchanged stretching frequency seem to be at variance with this argumentation but this dependence can be explained by a *kinematic* effect due to the increasing size of the benzene ring and thus increasing moments of inertia of the monomer upon electronic excitation. Considering the vdW bending mode as a librational mode[51,22] with a (hindered) internal rotation of the monomer within the complex, the decrease of the bending frequency upon electronic excitation becomes clear as has been shown in Ref. 21. Using the classical formula for the bending frequencies $\nu_{bend}\sim(1/\mu+r^2/I_b)^{22}$ with the B rotational constants of benzene derived in our previous work[43] (I_b is the in-plane moment of inertia of benzene, μ the reduced mass, and r the distance of the rare gas atom from the center of mass of benzene) we obtain $\nu_{bend}(S_0)/\nu_{bend}(S_1)=1.025$, i.e., a *decrease* of the bending frequency by $\approx 2.5\%$ upon electronic excitation. This is in reasonable agreement with the experimentally observed decrease of $\approx 4\%$ (see above). The experimentally detected change of vdW *vibrational* frequencies upon electronic excitation demonstrates that experimental results for the S_1 state cannot be directly compared with theoretical results from quantum mechanical bound state calculations performed for the S_0 state. Table III compares the new experimental results for the S_0 state with theoretical results for this state. It demonstrates agreement between theoretical and experimental (CIS) data at a satisfying level. The theoretical values are taken from a 3D quantum mechanical calculation[31] based on the Morse-fit to an *ab initio* potential.[54] The experimental data presented in this work may be the basis for critical comparison with theoretical results leading to an improvement of the theoretical intermolecular potential.

In conclusion, we presented the rotationally resolved spectrum of the vdW modes of ground state benzene-Ar up to an intermolecular energy of 130 cm^{-1}. We have been able to detect the corresponding weak bands using the new technique of coherent ion dip spectroscopy (CIS). Benzene–Ar is particularly suitable for CIS experiments because the perpendicular rotational band structure of the vdW vibronic bands with individual rotational lines allows one to select single rotational transitions for the pump transition. This is inevitable for a CIS experiment which is based on the selection of an effective three-level system. While in benzene–Ar only three vdW vibronic bands have been detected up to 63 cm^{-1} intermolecular energy in the $S_1\leftarrow S_0$ spectrum,[4,44] the high sensitivity of the CIS method enabled us to detect more than 7 vdW vibrational states in the S_0 state of the benzene–Ar complex up to 130 cm^{-1} intermolecular energy; six of these states have not been detected before.

An important future goal of CIS experiments is to determine the rotational constants of the ground state vdW levels. For this various CIS spectra of each vdW vibrational state using several different selected upper rovibronic levels have to be measured. In this way, information about vibration–rotation coupling will be obtained and directions and amplitudes of the intermolecular motions can be derived and compared with results from recent theoretical approaches.

ACKNOWLEDGMENTS

[1] For a review, see H. J. Neusser and R. Sussmann, in *Jet Spectroscopy and Molecular Dynamics*, edited by J. M. Hollas and D. Phillips (Chapman and Hall, London, 1995).

[2] J. A. Menapace and E. R. Bernstein, J. Phys. Chem. **91**, 2533 (1987).

[3] S. Leutwyler and J. Bösiger, Chem. Rev. **90**, 489 (1990).

[4] H. J. Neusser, R. Sussmann, A. M. Smith, E. Riedle, and Th. Weber, Ber. Bunsenges. Phys. Chem. **96**, 1252 (1992).

[5] W. Scherzer, H. L. Selzle, and E. W. Schlag, Chem. Phys. Lett. **195**, 11 (1992).

[6] M. Schmidt, J. Le Calve, and M. Mons, J. Chem. Phys. **98**, 6102 (1993).

[7] C. A. Haynam, D. V. Brumbaugh, and D. H. Levy, J. Chem. Phys. **80**, 2256 (1984).

[8] W. M. van Herpen, W. L. Meerts, and A. Dynamus, J. Chem. Phys. **87**, 182 (1987).

[9] B. B. Champagne, D. F. Plusquellic, J. F. Pfanstiel, D. W. Pratt, W. M. van Herpen, and W. L. Meerts, Chem. Phys. **156**, 251 (1991).

[10] Th. Weber, A. von Bargen, E. Riedle, and H. J. Neusser, J. Chem. Phys. **92**, 90 (1990).

[11] R. Sussmann, R. Neuhauser, and H. J. Neusser, Can. J. Phys. **72**, 1179 (1994).

[12] J. C. Alfano, S. J. Martinez III, and D. H. Levy, J. Chem. Phys. **94**, 1673 (1991).

[13] Th. Weber and H. J. Neusser, J. Chem. Phys. **94**, 7689 (1991).

[14] R. Sussmann and H. J. Neusser, Chem. Phys. Lett. **221**, 46 (1994).

[15] R. Sussmann, U. Zitt, and H. J. Neusser, J. Chem. Phys. **101**, 9257 (1994).

[16] R. Sussmann, R. Neuhauser, and H. J. Neusser, Chem. Phys. Lett. **229**, 13 (1994).

[17] R. Sussmann and H. J. Neusser, J. Chem. Phys. **102**, (1995).

[18] R. C. Cohen and R. J. Saykally, J. Phys. Chem. **94**, 7991 (1990).

[19] C. A. Schmuttenmaer, J. G. Loeser, and R. J. Saykally, J. Chem. Phys. **101**, 139 (1994).

[20] M. J. Elrod, R. J. Saykally, A. R. Cooper, and J. M. Hutson, Mol. Phys. **81**, 579 (1994).

[21] V. A. Venturo and P. M. Felker, J. Phys. Chem. (1993).

[22] P. M. Maxton, M. W. Schaeffer, S. M. Ohline, W. Kim, V. A. Venturo, and P. M. Felker, J. Chem. Phys. **101**, 8391 (1994).

[23] M. T. Berry, M. R. Brustein, M. I. Lester, C. Chakravarty, and D. C. Clary, Chem. Phys. Lett. **178**, 301 (1991).

[24] R. J. Stanley and A. W. Castleman, Jr., J. Chem. Phys. **94**, 7744 (1991).

[25] R. Sussmann, R. Neuhauser, and H. J. Neusser, J. Chem. Phys. **100**, 4784 (1994).

[26] Th. Brupbacher and A. Bauder, Chem. Phys. Lett. **173**, 435 (1990).

[27] Th. Brupbacher, J. Makarewicz, and A. Bauder, J. Chem. Phys. **101**, 9736 (1994).

[28] D. E. Cooper, C. M. Klimcak, and J. E. Wessel, Phys. Rev. Lett. (1981).

[29] M. Ito, Int. Rev. Phys. Chem. **8**, 147 (1989).

[30] R. Neuhauser, R. Sussmann, and H. J. Neusser, Phys. Rev. Lett. **74**, 3141 (1995).

[31] A. van der Avoird, J. Chem. Phys. **98**, 5327 (1993).

[32] C. E. Hamilton, J. L. Kinsey, and R. W. Field, Annu. Rev. Phys. Chem. **37**, 493 (1986).

[33] For a review, see J. Opt. Soc. Am. B **7**, (1990).

[34] E. Riedle, R. Moder, and H. J. Neusser, Opt. Commun. **43**, 388 (1982).

[35] G. Alzetta, A. Gozzini, L. Moi, and G. Orriols, Nuovo Cimento Soc. Ital. Fis. **36**B, 5 (1976); R. M. Whitley and C. R. Stroud, Phys. Rev. A **14**, 1498 (1976); C. Cohen-Tannoudji and S. Reynaud, J. Phys. B **10**, 2311 (1977); S. Swain, J. Phys. B **15**, 3405 (1982); P. M. Radmore and P. L. Knight, J. Phys. B **18**, 561 (1982); F. T. Hioe and C. E. Carrol, Phys. Rev. A **37**, 3000 (1988); C. Mavroyannis, Quantum Opt. **4**, 109 (1992).

[36] A. Messiah, *Quantenmechanik* (de Gruyter, Berlin, 1985), Vol. 2, p. 226 ff.

[37] U. Gaubatz, P. Rudecki, S. Schiemann, and K. Bergmann, J. Chem. Phys. **92**, 5363 (1990); G. W. Coulston and K. Bergmann, *ibid.* **96**, 3467 (1992).

[38] A. Kuhn, G. W. Coulston, G. Z. He, S. Schiemann, and K. Bergmann, J. Chem. Phys. **96**, 4215 (1992).

[39] S. Schiemann, A. Kuhn, S. Steuerwald, and K. Bergmann, Phys. Rev. Lett. **71**, 3637 (1993).

[40] D. Grischkowsky and M. M. T. Loy, Phys. Rev. A **12**, 1117 (1975).

[41] N. Dam, L. Oudejans, and J. Reuss, Chem. Phys. **140**, 217 (1990); J. Oreg, F. T. Hioe, and J. H. Eberly, Phys. Rev. A **29**, 690 (1984); B. Broers, H. B. van Linden van den Heuvell, and L. D. Noordam, Phys. Rev. Lett. **69**, 2062 (1992).

[42] V. S. Letokhov and V. P. Chebotayev, in *Nonlinear Laser Spectroscopy, Springer Series in Optical Sciences*, edited by D. L. MacAdam (Springer, Berlin, 1977), Vol. 4.

[43] E. Riedle, Th. Knittel, Th. Weber, and H. J. Neusser, J. Chem. Phys. **91**, 4555 (1989).

[44] E. Riedle, R. Sussmann, Th. Weber, and H. J. Neusser, J. Chem. Phys. (submitted).

[45] J. H. Callomon, T. M. Dunn, and I. M. Mills, Philos. Trans. R. Soc. London Ser. A **259**, 499 (1966).

[46] J. T. Hougen, J. Chem. Phys. **37**, 1433 (1962).

[47] A. R. Hoy and I. M. Mills, J. Mol. Spectrosc. **46**, 333 (1973).

[48] A. B. Hollinger and H. L. Welsh, Can. J. Phys. **56**, 1513 (1978).

[49] Th. Weber, E. Riedle, and H. J. Neusser, J. Opt. Soc. Am. B **7**, 1875 (1990).

[50] G. Herzberg, *Molecular Spectra and Molecular Structure* (Van Nostrand, Princeton, 1966), Vol. III, Chap. II.3.

[51] M. Mons and J. Le Calvé, Chem. Phys. **146**, 195 (1990).

[52] E. Riedle and A. van der Avoird, J. Chem. Phys. (submitted).

[53] G. Brocks and D. van Koeven, Mol. Phys. **63**, 999 (1988).

[54] P. Hobza, H. L. Selzle, and E. W. Schlag, J. Chem. Phys. **95**, 391 (1991).

[55] G. Herzberg, *Molecular Spectra and Molecular Structure* (Van Nostrand, New York, 1945), Vol. II, p. 421 ff.